

Supplementary Information for

“Elucidating Mysteries of Phase-Segregated Membranes: Mobile-Lipid Recruitment Facilitates Pores’ Passage to the Fluid Phase”

Jesús M. López Martí,¹ Niall J. English² and Mario G. Del Pópolo^{1,3} *

¹*CONICET & Facultad de Ciencias Exactas y Naturales, Universidad Nacional de Cuyo, Padre Jorge Contreras 1300, CP5500, Mendoza, Argentina.*

²*School of Chemical and Bioprocess Engineering, University College Dublin, Belfield, Dublin 4, Ireland.*

³*Atomistic Simulation Centre, School of Mathematics and Physics, Queen's University Belfast, University Road, Belfast BT7 INN, UK.*

Table of contents:

1. **Figure S1:** Local composition across a phase-segregated dipalmitoyl-phosphatidylcholine (DPPC):dilinoleyl-phosphatidylcholine (DIPC):cholesterol (CHOL), membrane.
2. The movie files **xi-0.8-phase-segregated-bilayer-top-view.mpg** and **xi-0.8-phase-segregated-bilayer-water-side-view.mpg** show the time evolution of the system (~2 μ s) after a pore ($\xi_0=0.8$, $R\sim 1$ nm) was created at the centre of the L_o domain. The bilayer is depicted from above. At some point, the pore moves across the periodic y-boundary of the simulation cell. Colour code: DPPC-DIPC-CHOL = Blue-Red-Yellow. The second movie shows a lateral view of the system along the y-axis. Only water molecules were included in the rendering, to emphasize the membrane surfaces and the drifting transmembrane water channel.
3. **Figure S2:** Pore radii as a function of time.
4. **Figure S3:** Time evolution of membrane excess area.
5. **Figure S4:** Time evolution of mismatch area between domains’ upper and lower leaflets.
6. **Figure S5:** Functional relationship between order parameter (ξ) and pore radius (R).
7. **Figure S6:** Difference in free energy cost for creating pores in the bulk of L_o or L_d phases, i.e $\Delta G_{L_d}(R) - \Delta G_{L_o}(R)$.
8. **Figure S7:** Least-square fittings to the Classical Nucleation Theory expression for the pore energy.

* Corresponding author: mdelpopolo@fcen.uncu.edu.ar & m.delpopolo@qub.ac.uk

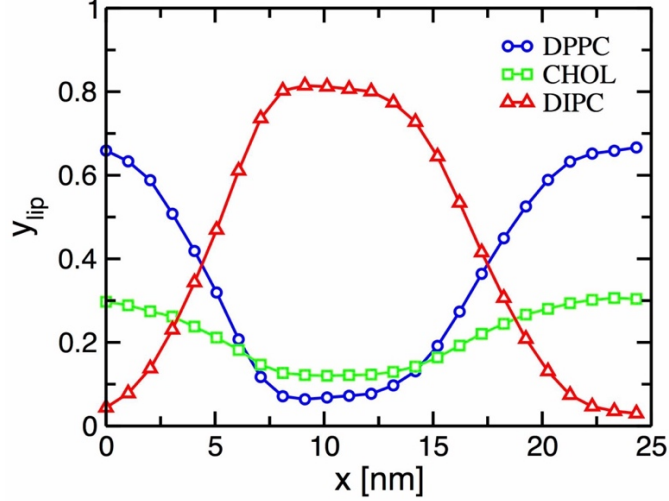


Figure S1: Membrane composition across a phase-segregated dipalmitoyl-phosphatidylcholine (DPPC), dinoleyl-phosphatidylcholine (DIPC), and cholesterol (CHOL) membrane (DPPC:DIPC:CHOL) at $T=295\text{K}$. The x -direction runs perpendicular to the domain borders; $y_{\text{lip}} = N_i / (N_{\text{DPPC}} + N_{\text{DIPC}} + N_{\text{Chol}})$. The DPPC-rich L_o domain has an average composition of (0.67:0.04:0.29). The DIPC-rich L_d domain has a composition of (0.07:0.81:0.12). As noticed by Risselada et al. a temperature of 295K is optimal to observe clear phase separation within accessible simulation time scales. A higher temperature brings the system closer to the critical point making the identification of phase domains much more difficult.

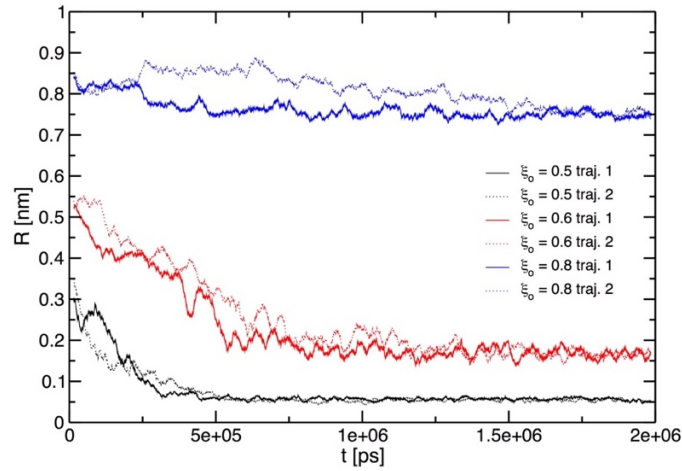


Figure S2: Pore radius, R , as a function of time for each of the 2 μs MD production runs reported in the paper. In all cases pores were created ($t=0$) at the centre of the L_o domain, on the final configuration of the 4 μs simulation of the phase-segregated membrane. In order to prevent spontaneous pore collapse, ξ_0 was harmonically restrained to the values annotated on the figure. Larger pores ($\xi_0=0.8$) do not change size when crossing the domain boundary, smaller pores do ($\xi_0=0.6, 0.5$). For $\xi_0=0.8$ and 0.6 pores are toroidal and hydrophilic, whether located in L_o or L_d , and a water channel crosses the bilayer. For $\xi_0=0.5$, the membrane defect is hydrophobic and amounts to a local lowering of the lipids density.

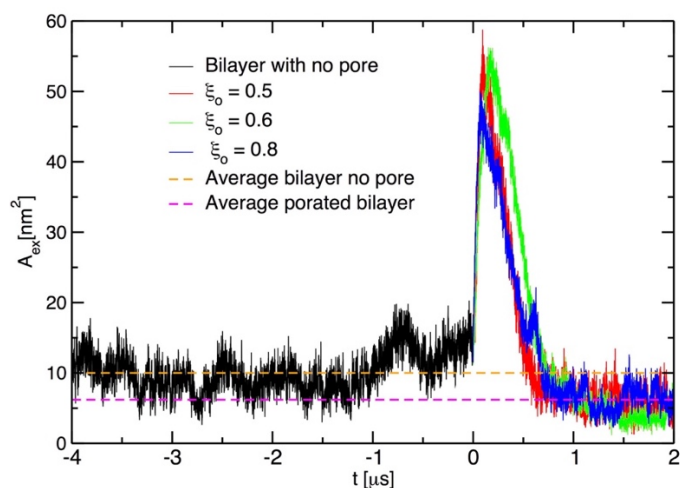


Figure S3: Time evolution of membrane excess area. The excess area is the difference between the actual surface area of the undulated membrane and the simulation box's X-Y area. The area of the undulated membrane was computed by fitting a geometric surface to the phosphate groups of DPPC and DIPC, as described in ref. 29, and implemented in g_lomepro.² This utility code also allowed us to correlate pore position with local membrane curvature. The black line (spanning negative times) corresponds to A_{ex} evaluated on the non-porated phase-segregated bilayer. Pores with $\xi_0=0.8$ (blue), $\xi_0=0.6$ (green), and $\xi_0=0.5$ (red), created at $t=0$, immediately induce membrane bending resulting in larger values of A_{ex} . The deformation relaxes as stress is released while the pores drift and reach the centre of the L_d phase.

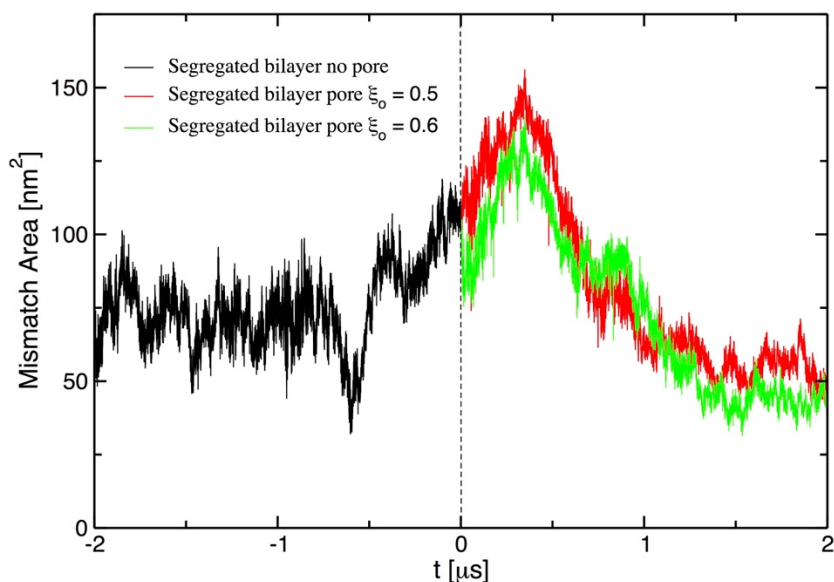


Figure S4: The mismatch area quantifies the overall extent to which the domains' upper and lower leaflets are out of kilter. The positive value shown by the non-porated

² http://www3.mpibpc.mpg.de/groups/de_groot/g_lomepro.html

membrane (black line) is due to a small surface tension that controls the degree of registration between the two domain leaflets (see ref. 3). Pores are created in L_o at $t=0$, inducing membrane curvature and pushing the upper and lower leaflets out of kilter. The mismatch area goes back to normal once the pores reach L_d . Only one trajectory for $\xi_0=0.6$ (green) and $\xi_0=0.5$ (red) is shown, the others depict similar trends.

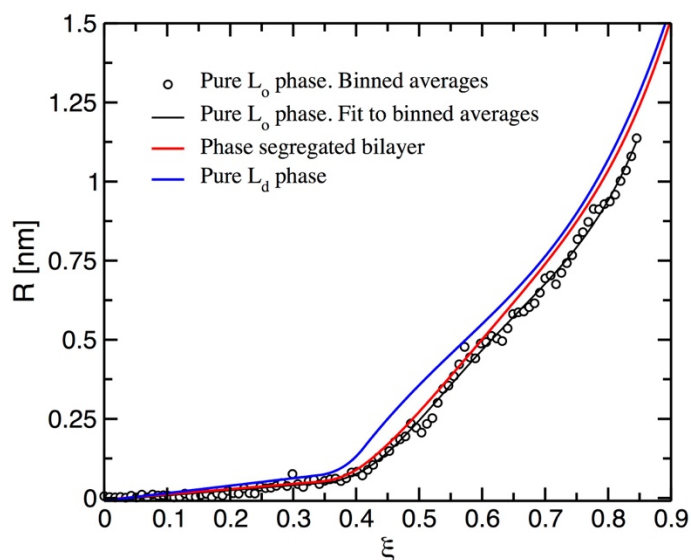


Figure S5: $R(\xi)$ functions computed by Monte Carlo (see paper) from the various simulated systems, as annotated on Figure.

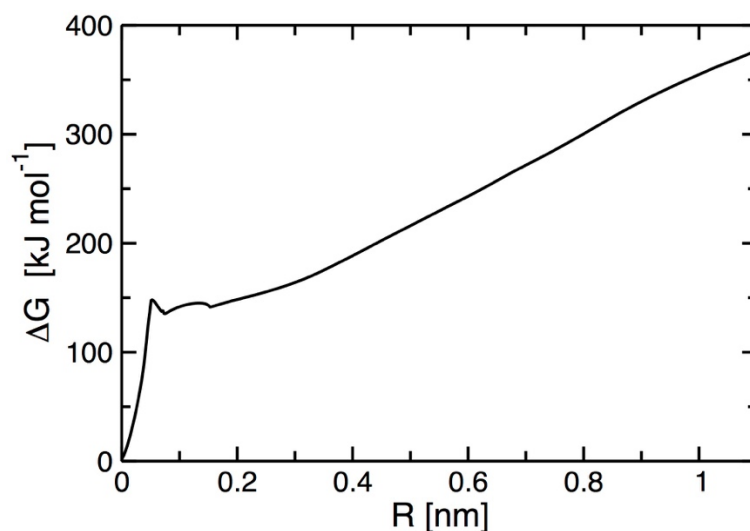


Figure S6: Difference in free energy cost for creating a pore of radius R in the bulk of L_o or L_d , i.e. $\Delta G(R) = \Delta G_{L_d}(R) - \Delta G_{L_o}(R)$. $-\Delta G(R)$ is the driving force that pushes the pore from L_o to L_d .

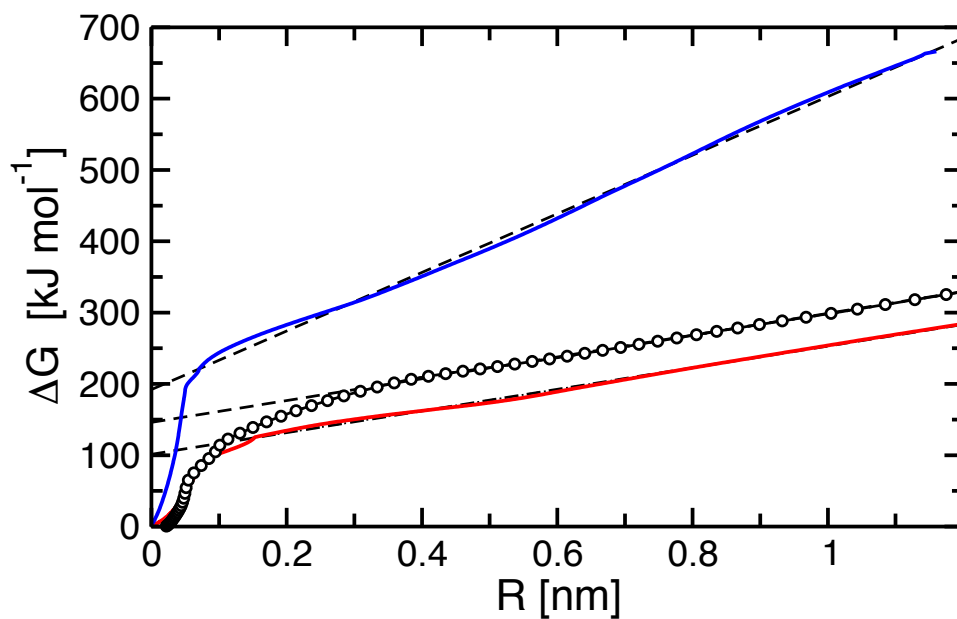


Figure S7: Free-energy vs. pore radius, as shown in the bottom panel of Figure 4. The dashed lines are least-square fittings to the Classical Nucleation Theory expression for the pore energy (equation 1 in the manuscript, with $\gamma_s = 0$) in the $R \in (0.3-1.3)$ nm interval. In each case, the ordinate of the origin provides ΔG_n , the slope allows to compute γ_L .